Chapter 2

Synthesis and Experimental Methods

The sample preparation method and characterization techniques used in the present thesis work are described in this chapter. The bulk polycrystalline systems of intermetallic compounds are prepared using the standard arc melting technique. The thin film of perovskite compound is prepared using the magnetron sputtering technique. The structural characterization of the prepared systems is done by using the laboratory and synchrotron x-ray diffractometer. The scanning electron microscope (SEM) equipped with the energy dispersive spectroscopy (EDS) detector is used for surface imaging and compositional study of the synthesized systems. In addition, x-ray photoelectron spectroscopy (XPS) and x-ray absorption near Edge spectroscopy (XANES) are used for the examination of light elements. The physical properties such as magnetization, AC-susceptibility, and resistivity are measured in the physical properties measurement system (PPMS). Some resistivity measurements have been performed in a cryogen-free measurement system (CFMS). The detailed working principle and procedures of these experimental techniques are discussed in this chapter.

2.1 Sample preparation

2.1.1 Arc-melting technique

Arc-melting is used to melt raw materials with at least 99.9% purity to form an alloy. The actual image of the arc melting setup with the vacuum sealing unit is shown in Fig. 2.1 (a). The heat for melting is generated by an arc generated in between the tungsten electrode and raw materials placed in a crucible in the Cu-hearth. Before melting, the arc furnace is evacuated by using a rotary pump and then filled with argon gas. Thus, the melting is performed in the argon atmosphere.

The arc melting setup consists of an arc furnace with four crucibles in the Cu-hearth [Fig. 2.1(b)], standard tungsten inert gas (TIG) welding unit (power supply) to feed electricity, a water chiller for the purpose of cooling to prevent equipment from burning out due to excess heat, and vacuum unit (rotary pump). Inside the arc furnace, we put the raw materials in one of the crucibles after weighing them in the right proportion to prepare a particular composition of the alloy. In addition, we put a Ti ball in another crucible. After that, we start the rotary pump and leave the system for at least one and a half hours to achieve a vacuum of around 10^{-3} mbar. Evacuation is followed by 4-5 times purging with argon gas to improve the vacuum more so that the raw material does not get oxidized

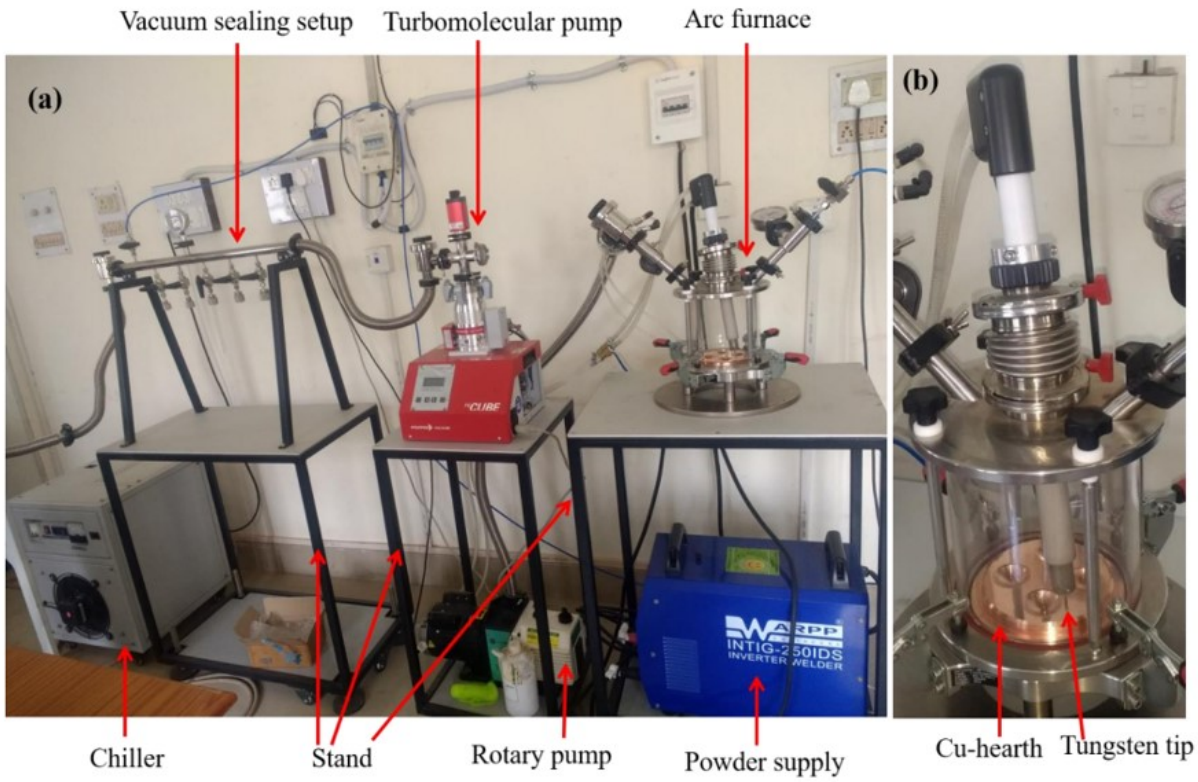

Figure 2.1: (a) Actual image of Arc Melting set up at the School of Materials Technology, IIT(BHU), Varanasi, India. (b) An enlarged view of the arc melting furnace.

during the melting. Purging is the process in which the chamber is first filled with argon gas up to atmospheric pressure and evacuated again. The heavy molecule of Ar gas facilitates the evacuation of air molecules from the arc chamber. After purging, we filled the argon gas up to $\sim$1 psi and started the water chiller, which helps to prevent the burning of the different components from excess heat during melting. The Ti ball, which is highly reactive to oxygen, was melted first to remove the remaining oxygen molecule in the atmosphere. The melting was done by the application of alternating current to the tungsten electrode, which is arranged such that it generates an arc discharge between the electrode and Cu-hearth inside the furnace. Subsequently, the melting of raw materials was done to prepare the sample. Generally, the melting is performed 3-4 times by flipping the sample to achieve a good homogeneous composition. The arcing generates such a high temperature ($\sim 3000^0$C) that raw materials containing metal can be melted evenly within a short time. This technology is also used in the field of steel making. The mass of material is measured after and before the melting. The weight loss after melting was found to be less than 2%. The ingot/sample, obtained after melting, was further annealed in a vacuum atmosphere to improve homogeneity. For

that, the sample was first sealed in a quartz tube after evacuating it up to the vacuum of around 10^{-6} mbar using the turbo molecular pump or diffusion pump. After that, the sealed quartz ampoule was annealed in the furnace at the required temperature and time, depending on the composition. Finally, the vacuum-sealed sample was slowly cooled or quenched in ice water depending on the required preparation condition to achieve the pure ordered phase.

2.1.2 Magnetron sputtering

Magnetron sputtering is the most widely used thin-film fabrication technology. It is a type of solid-source ion plating technology. This technique provides a high deposition rate as compared to the conventional direct current (DC) sputtering technique, as well as forms a dense coating on the substrate. It is because of the fact that it utilizes a magnetic field to trap the secondary electrons near the target, which is generated due to bombardment on the target.

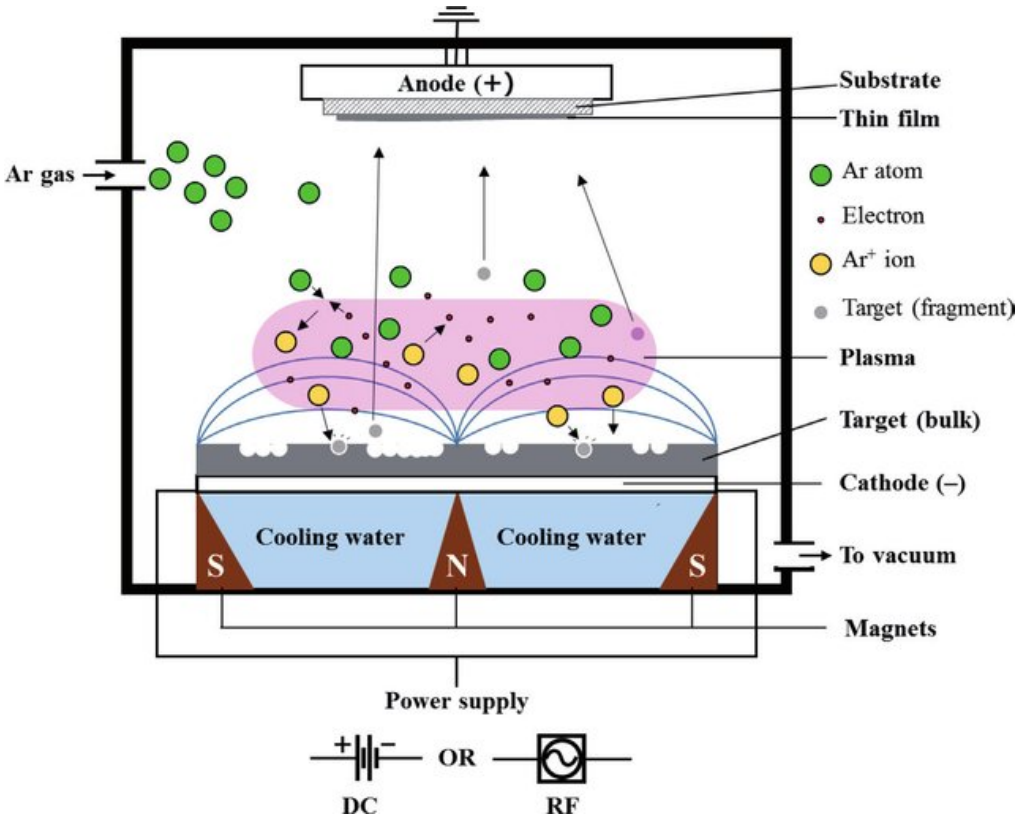

Figure 2.2: Schematic representation of a magnetron sputtering equipment and deposition process [1].

In this way, it creates dense plasma near the target. Generally, argon (Ar) gas is used as a working gas for bombardment purposes because it is an inert gas. Ar ions are accelerated and collide with

the target surface to eject target atoms. Then the sputtered atoms are condensed into a film on the substrate. The major components of magnetron sputtering are an ultra-high vacuum (UHV) compatible chamber, magnetron source (target material), DC/RF power supply, etc.

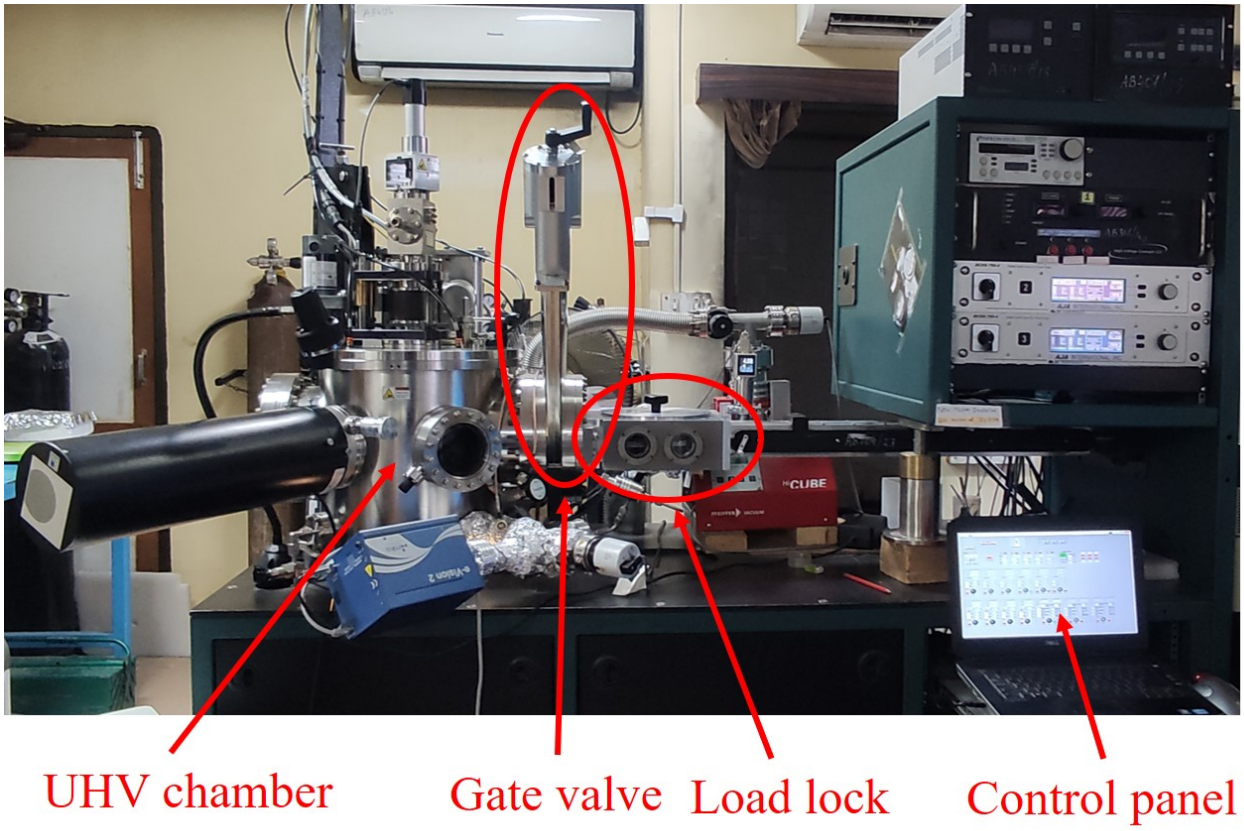

Figure 2.3: Actual image of DC magnetron sputtering, available at UGC-DAE CSR, Indore.

The Magnetron sputtering works on the principle when power is supplied to a magnetron, a negative voltage of typically −300 V or more is applied to the target; this negative voltage attracts Ar^+ ions to the target surface, inducing large kinetic energy at the same time. It is well known that an energy transfer occurs when Ar^+ collides with atoms at the surface. If the energy transferred to a lattice site is greater than the binding energy, primary recoil atoms can be created, which can further collide with other atoms and distribute their energy via collision. Sputtering occurs if the energy transferred to the target surface is larger than about three times the surface binding energy. Here, the target is kept as a cathode, whereas the substrate acts as an anode. The emitted target atoms are then directed toward the substrate. However, in this process, further secondary electrons are created, which are confined due to the magnetic field and eventually reinforce the process of ionization of the Ar atoms. This results in the formation of dense and uniform thin films. Schematic representation of a magnetron

sputtering equipment and deposition process is shown in Fig. 2.2.

The thin film system was deposited using the direct current magnetron sputtering technique. The 2-inch and 3-inch targets were sputtered using Ar (99.9995% purity). The base pressure of 1.2×10^{-7} Torr or lower was achieved before deposition. The working pressure was about 2.4 mTorr due to the flow of process gases. The actual image of DC magnetron sputtering is shown in Fig. 2.3, available at UGC-DAE CSR, Indore.

2.2 Structural characterization

2.2.1 Powder x-ray diffractometer

In powder X-ray diffractometer (XRD) available in the laboratory, the diffraction pattern is obtained from a powder of the material, rather than an individual crystal. The powder x-ray diffractometer is widely used for phase identification of a crystalline material and can provide information on unit cell dimensions, atomic structure, crystallite size, microstrain, etc. Max von Laue, in 1912, discovered that crystalline substances act as three-dimensional diffraction gratings for X-ray wavelengths, and each crystal has its own unique XRD pattern [2]. XRD is based on constructive interference of monochromatic x-rays. The interaction of the incident rays with the sample produces constructive interference (and a diffracted ray) [Fig. 2.4] when conditions satisfy Bragg′s Law-

$$n\lambda = 2dsin\theta \tag{2.1}$$

where d, θ, λ, and n are interplanar spacing, incident/Bragg angle of x-ray on the sample, the wavelength of x-ray, and order of reflection, respectively. The powder X-ray diffractometer (Rigaku, model no. RINT 2500/PC series) consists of an x-ray source (usually an x-ray tube), a water chiller to cool the X-ray tube, a detector, and a sample stage with a goniometer to measure the angle inclined by the detector with respect to the incident x-ray. The x-ray with a maximum power of 6 kW is generated by the x-ray tube, filtered to produce monochromatic radiation, collimated to concentrate, and directed toward the sample. Copper is the target material used in the diffractometer, with

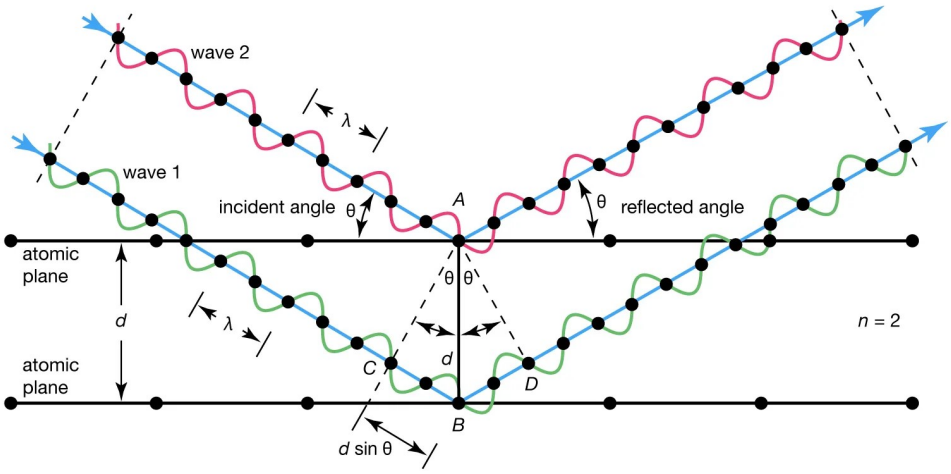

Figure 2.4: Bragg′s law [3].

Cu-K_α radiation = 1.54 Å. The x-ray is focused on the sample at some angle θ, while the detector opposite the source reads the intensity of the x-ray, which it receives at 2θ away from the direction of the incident ray.

The 2θ is then increased over time with respect to the incident ray to collect all the possible reflections from the planes with different d present in the crystalline system. In general, powder diffraction patterns have been collected at 2θ from $\sim 20^\circ$ to 120° with the scan rate 2°/minute. It also consists of low-temperature (up to 10 K) and high-temperature attachment (up to 1200°C), which facilitate the study of temperature-dependent structural change. The He-based cryostat is used to achieve low temperatures, whereas the heater is for high temperatures. In both regions, it should make sure that the environment has been properly evacuated. For that purpose, there is the arrangement of rotary and turbomolecular pumps. This diffractometer works in the Bragg-Brentano geometry. The actual picture of the powder x-ray diffractometer is given in Fig. 2.5

2.2.2 Synchrotron x-ray powder diffractometer (SXRPD)

SXRPD offers better sensitivity and resolution of diffraction peaks than conventional laboratory powder XRD because of high energy flux, tunable well-defined wavelength, and better collimation of synchrotron radiation in order to collect information about small changes in the crystal structure. Similar to conventional laboratory XRD, SXRD works on the principle of Bragg′s law. A synchrotron primarily consists of an electron gun, linear accelerator (linac), circular shape vacuum

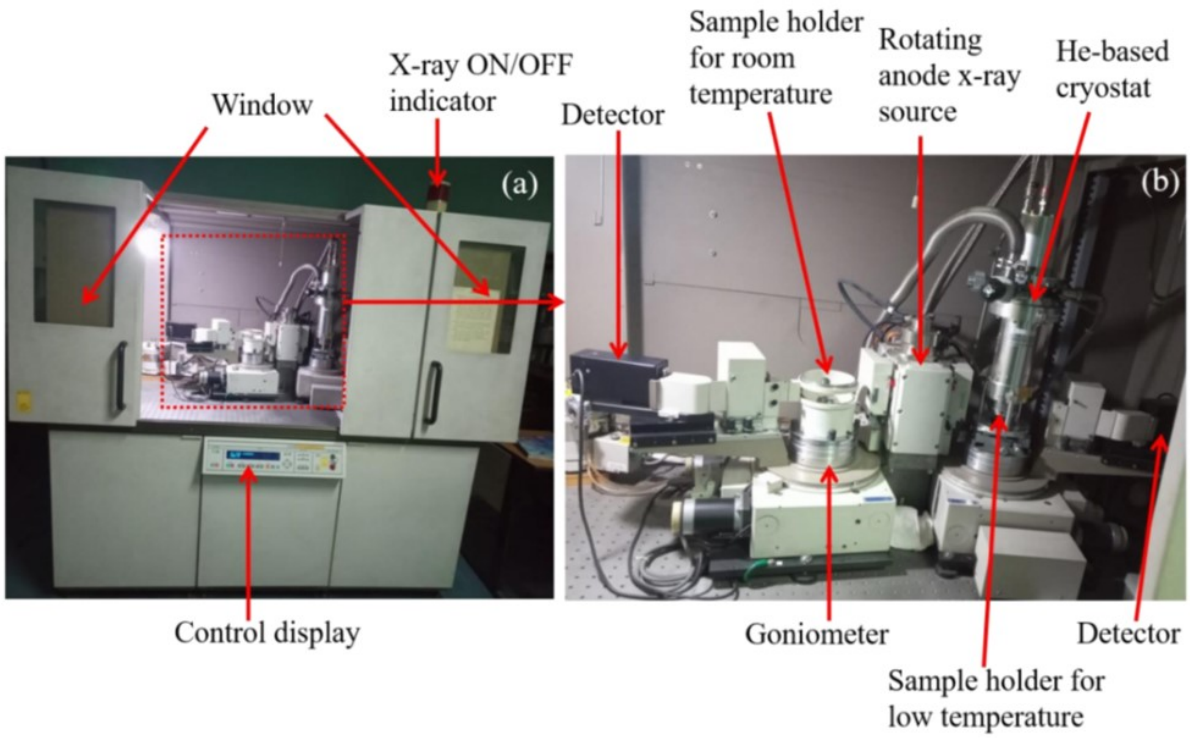

Figure 2.5: Actual image of the Rigaku x-ray diffractometer present at the School of Materials Technology, IIT (BHU), Varanasi, India.

tubes with circumferences of up to several hundred meters (booster and storage rings), bending magnet, focusing magnet, and experimental station, as shown in Fig. 2.6. Once electrons are generated from the electron gun, they pass through the linac to attain the speed close to the speed of light. Then, these electrons are transferred to the booster ring to boost their energy before transferring to the storage ring. the storage ring consists of a series of magnets separated by straight sections that allow the electrons to circulate around the ring. Electromagnetic radiation (synchrotron light with a wide-spectrum range covering from microwaves to hard X-rays) is generated as a result of the deflection of the electrons in the magnetic field created by the bending magnets. The intensity of the synchrotron light can be significantly increased by placing an insertion device (wiggler or undulator) in the straight sections of the ring.

In the beamline, high-intensity synchrotron radiation is modulated by a series of slits, filters, and various X-ray optical components such as monochromator devices, silicon crystals with focusing bent elements mirrors, and refraction elements as it leaves the storage ring through a guided shielded end. The user can select the wavelength required for the experiment either with a suitable monochromator

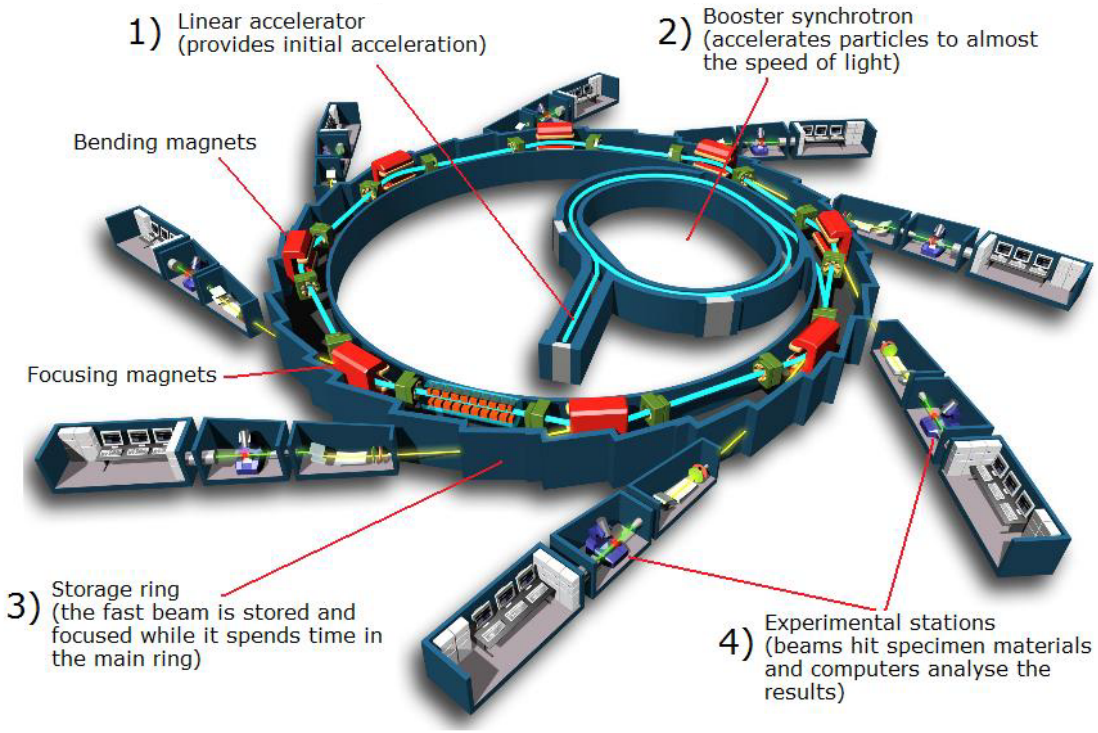

Figure 2.6: General representation of synchrotron to produce monochromatic X-ray radiation [4].

or by adjusting the emission wavelength of the insertion devices. There is also a cooling system to regulate the excessive heat load during the experiment. A basic layout of a synchrotron to produce monochromatic X-ray radiation is shown in Fig. 2.6.

The synchrotron light sources, namely PETRA-III, were used for the SXRPD measurements. The SXRPD pattern was collected using high energy (60 keV) x-rays with wavelength $\lambda \sim 0.207$ at P02.1 beamline of PETRA-III, DESY, Hamburg, Germany. The schematic diagram of the P02.1 beamline of PETRA-III is given in Fig. 2.7 (a), where the path of the x-ray from the undulator to the detector via the sample is shown.

The borosilicate capillaries were used as sample holders for the SXRPD measurements. The fine powder sample was packed in the borosilicate capillaries, spinning continuously during measurement to minimize the texturing effect in the SXRPD data. A actual image of the mounted capillary ready for diffraction measurement is depicted in Fig. 2.7 (b). The SXRPD data was collected in the transmission mode based on the Debye-Scherrer principle using a 2D detector (Perkin Elmer, 200×200 μm^2 pixel size). The high-resolution SXRPD data were collected by moving the 2D detector away from the sample (sample to detector distance sim1200-1500 mm). The high-Q data for

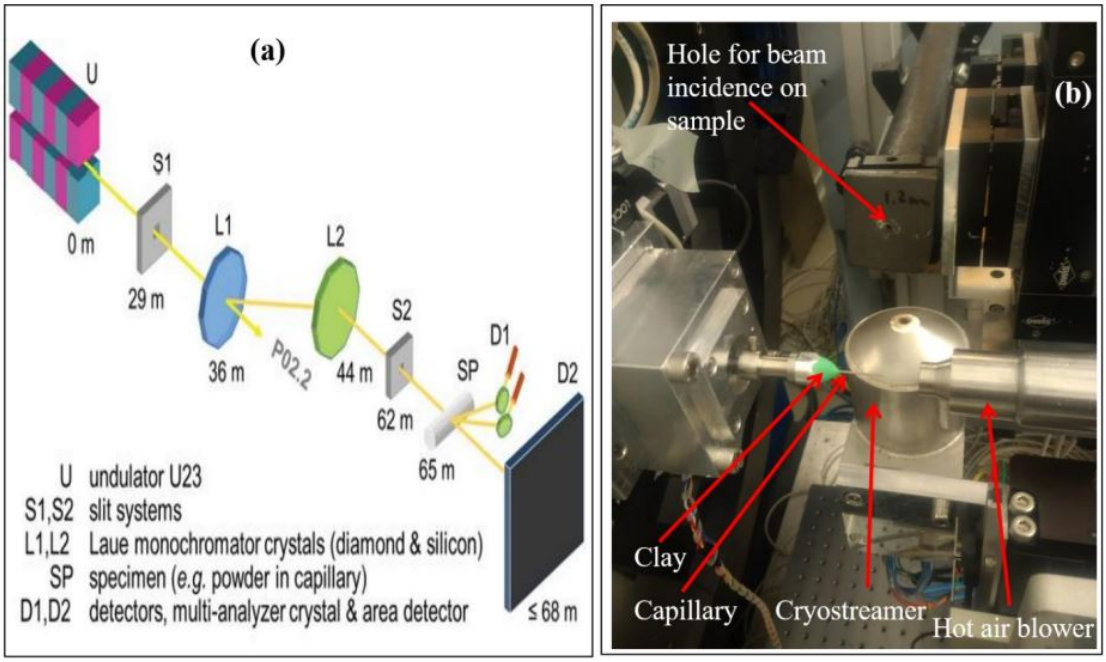

Figure 2.7: (a) Schematic diagram of optics of P02.1 beamline of PETRA-III, DESY [5]. (b) Actual image of mounted capillary during measurement at P02.1 beamline of PETRA-III, DESY.

empty borosilicate capillaries were also collected to remove the background contribution from the diffraction data of the sample. For the temperature variation (100-400 K), a nitrogen cryo steamer was used directly to the capillary. The raw 2D image data were integrated into 1D diffraction (Intensity versus 2θ) using the program Fit2D and Dawn Diamond.

2.3 Magnetic measurement

Physical property measurement system (PPMS) with vibrating sample magnetometer (VSM)

The DynaCool physical property measurement system (PPMS), which is a cryogen-free system, is used to measure the material properties like specific heat, magnetization, AC susceptibility, and electrical transport properties in an environment where the magnetic field and temperature are well-controlled. The type of materials used for measurement should be typically in bulk, thin film, and powder form. Powders are typically pressed into geometries that satisfy the dimensional require-

ments.

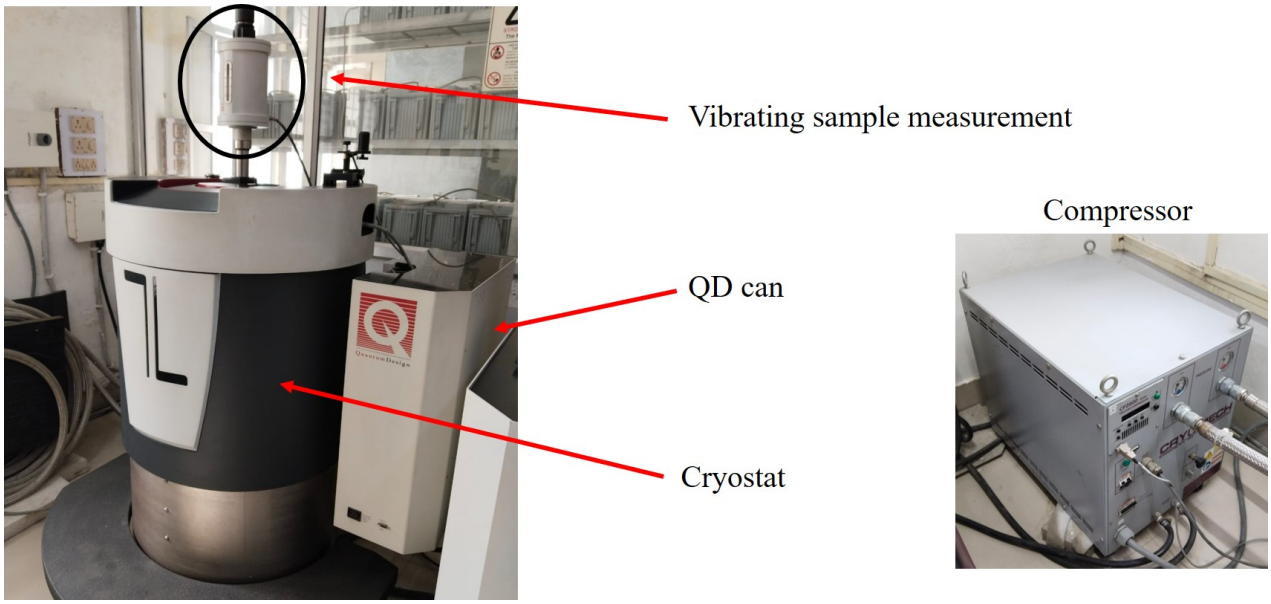

Figure 2.8: Actual image of physical property measurement system available at the School of Materials Technology, IIT (BHU), Varanasi, India.

The PPMS can be used with specially-designed measurement options or can be easily adapted to the required experiments. The base unit of the PPMS consists of a cryostat with a superconducting magnet coil. The cryostat utilizes a cold head with the compressor to cool down and reach cryogenic temperatures. Helium gas is needed to cool down both the sample chamber as well as the superconducting magnet coil and purge the sample chamber. The temperature can be varied continuously between 1.9 K and 400 K, while a magnetic field of upto ± 9 T can be applied. The different measurement options result from the use of different measurement inserts or sample holders and activating the according software mode. The actual image of PPMS is shown in Fig. 2.8.

The VSM option in PPMS measures the magnetization and AC susceptibility of the sample. The magnetic measurement is carried out by oscillating the sample near a gradiometer detection (pickup) coil and synchronously detecting the voltage induced. The VSM option for the PPMS consists of a VSM linear motor transport (head) for vibrating the sample, coilset puck for detection, electronics for driving the linear motor transport and detecting the response from the pickup coil, and a copy of the MultiVu software application for automation and control. The principle of operation for VSM is that a changing magnetic flux will induce a voltage in a pickup coil, which is based on Faraday′s

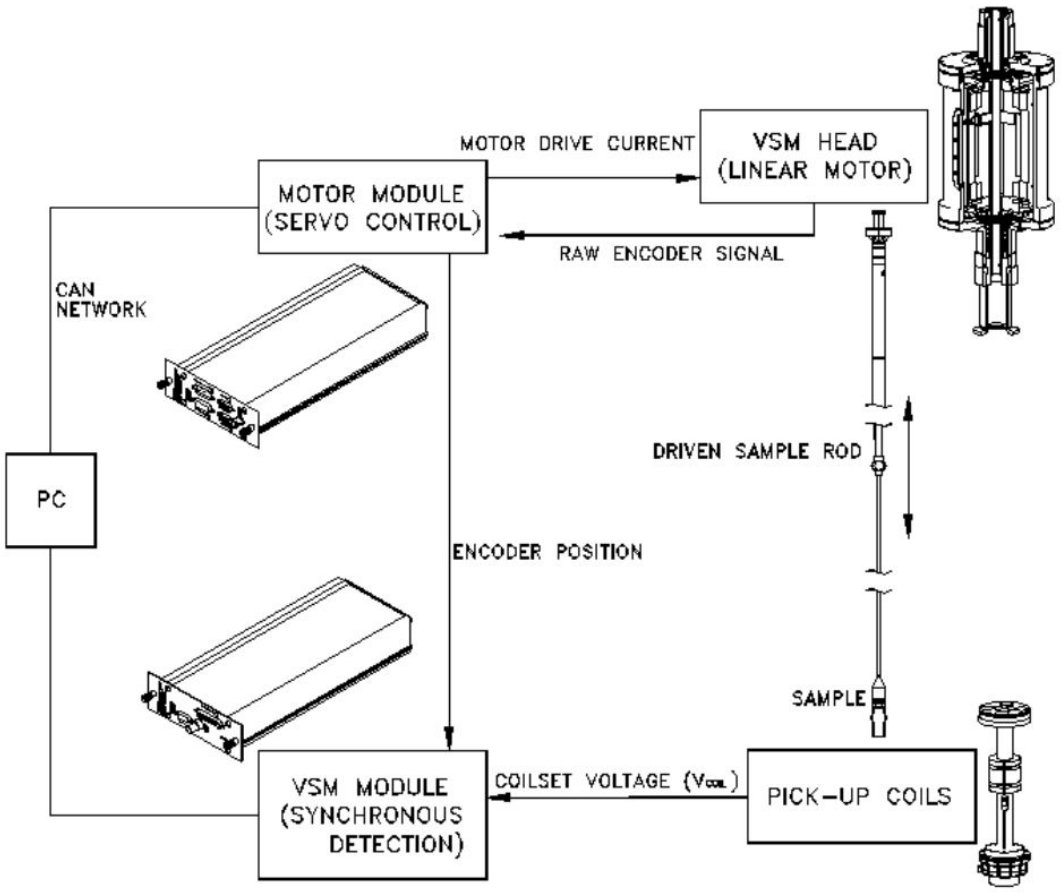

Figure 2.9: Schematic diagram of this measurement process with Physical property measurement system with a vibrating sample magnetometer [6].

law. The time-dependent induced voltage is given as follows-

$$V_{coil} = \frac{d\phi}{dt} = \frac{d\phi}{dz} \times \frac{dz}{dt} \tag{2.2}$$

where ϕ is the magnetic flux enclosed by the pickup coil, z is the vertical position of the sample with respect to the coil, and t is time. For a sinusoidally oscillating sample position, the voltage can be expressed as-

$$V_{coil} = 2\pi f C m A Sin(2\pi f t) \tag{2.3}$$

where C is a coupling constant, m is the DC magnetic moment of the sample, A is the amplitude of oscillation, and f is the frequency of oscillation. The amplitude of the sinusoidal voltage response is used to measure the magnetic moment of the sample. The detailed schematic diagram of this measurement process with PPMS VSM is shown in Fig 2.9. The VSM has a sensitivity of $<10^{-6}$

emu, i.e., it is able to resolve magnetization changes of less than 10^{-6} emu. A typical operating condition is 2 mm peak amplitude and 40 Hz oscillating frequency. For magnetic measurement, the diametrical extent of the sample should be less than 4.5 mm and the length a few millimeters. The sample mass should be less than 10 mg for a highly magnetic one.

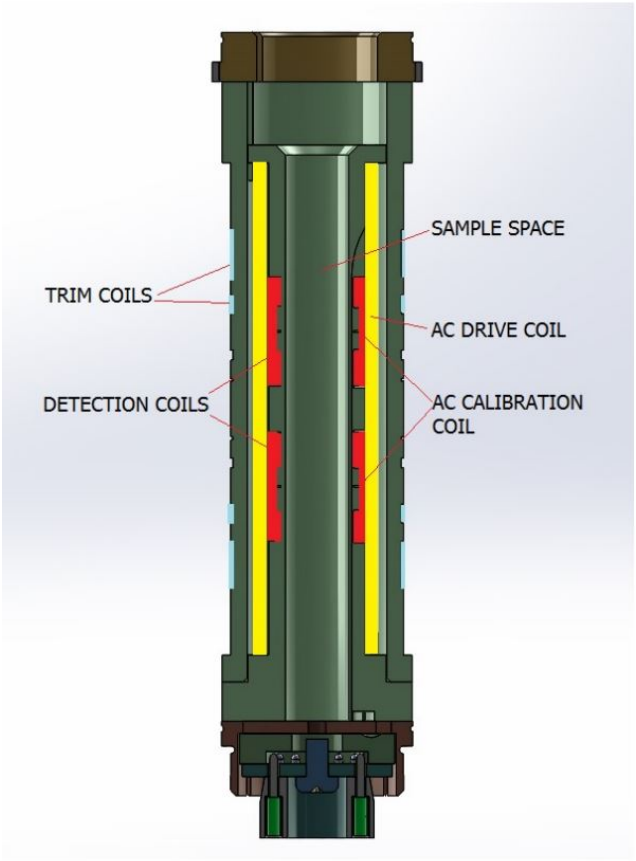

Figure 2.10: Schematic diagram of the ACMS II coil set.

The Quantum Design AC Measurement System (ACMS II) option for the PPMS is a versatile susceptometer. The measurement of AC magnetic susceptibility is based on the principle of mutual inductance for frequencies between 10 and 10,000 Hz. To understand the working principle of AC magnetometry, first consider very low frequencies (e.g., 1 Hz), where the measurement is most similar to DC magnetometry. In this case, the magnetic moment of the sample follows the magnetization versus magnetic field [M(H)] curve that would be measured in a DC experiment. As long as the AC field is small, the induced AC moment is $M_{AC} = (\frac{dM}{dH}) \cdot H_{AC} \sin(\omega t)$ where H_{AC} is the amplitude of the driving field, ω is the driving frequency, and $\chi = \frac{dM}{dH}$ is the slope of the M(H) curve, called the susceptibility. The susceptibility is the quantity of interest in AC magnetometry. As the applied DC magnetic field is changed, different parts of the M(H) curve are accessed, giving a different suscepti-

bility. One advantage of the AC measurement is the measurement is very sensitive to small changes in M(H). Since the AC measurement is sensitive to the slope of M(H) and not to the absolute value, small magnetic shifts can be detected even when the absolute moment is large.

At higher frequencies, the AC moment of the sample does not necessarily match the DC magnetization curve, due to dynamic effects in the sample, which is the reason it is known as dynamic susceptibility. In this higher-frequency case, the magnetization of the sample may lag behind the drive field. Thus, the AC magnetic susceptibility measurement yields two quantities- the magnitude of the susceptibility, χ, and the phase shift, ϕ (relative to the drive signal). In other words, the susceptibility has two components- an in-phase (or real) component χ' and an out-of-phase (or imaginary) component χ''. The two representations are-

$$\chi' = \chi Cos\phi, \chi' = \chi Sin\phi \tag{2.4}$$

In the limit of low frequency, the real component χ' is just the slope of the M(H) curve. The imaginary component, χ'', indicates dissipative processes in the sample. In conductive samples, the dissipation is due to eddy currents. The typical measurement that is performed is χ vs. DC field bias. The sample undergoes a three-point measurement process that utilizes the calibration coils in order to increase measurement accuracy. The first reading is made with the sample positioned at the center of the bottom detection coil. The sample is then re-positioned to the center of the top detection coil, and a second reading is taken. A third reading is made with the sample back at the center of the bottom coil. The three-point measurement provides the comparison of the sum of the two bottom coil signals with the two times of the top coil signal. This helps to correct for drifts in the sample moment and background throughout the measurement. A schematic diagram of the ACMS II coil set is shown in Fig. 2.10, wherein different coil sets are indicated. The ac drive amplitude and frequency were optimized for every measurement.

2.4 Resistivity measurement

2.4.1 Cryogen-free measurement system (CFMS)

The cryogen-free measurement System (CFMS) from Cryogenic Ltd. is a research system designed to perform a wide range of material characterization experiments, such as electrical transport measurements in variable magnetic fields and variable temperature environments. The system consists of a sample holder, a cryogen-free superconducting magnet with a variable temperature insert (VTI), compressor, etc. The actual picture of the CFMS system is shown in Fig. 2.11 (a).

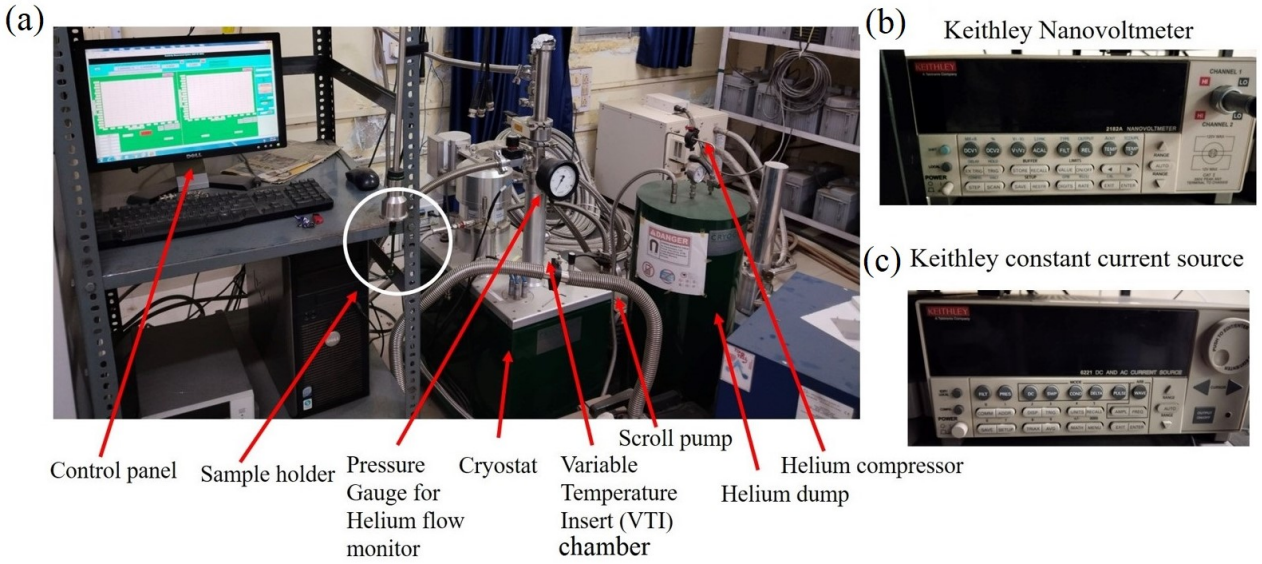

Figure 2.11: Actual image of cryogen-free measurement system available at the School of Materials Technology, IIT (BHU), Varanasi, India.

An automatic needle valve is supplied as standard for ease of system control. The maximum magnetic field and the lowest temperature can be achieved up to 7 T and 1.4 K, respectively. It does not facilitate high-temperature measurement. In the process to achieve the temperature around 1.4 K, we first evacuate the path from VTI chamber to the needle valve and from the needle valve to the helium inlet by using a scroll pump (dry pump) and rotary pump, respectively. To achieve a better vacuum, we left the system on evacuation for 2-3 days. Then, we attached the helium dump to the VTI chamber through the helium inlet and opened the needle valve to evacuate the whole path from the helium dump to VTI chamber using the scroll pump and left the system for the whole night.

Subsequently, the purging of the whole path is done by filling the helium dump with helium gas

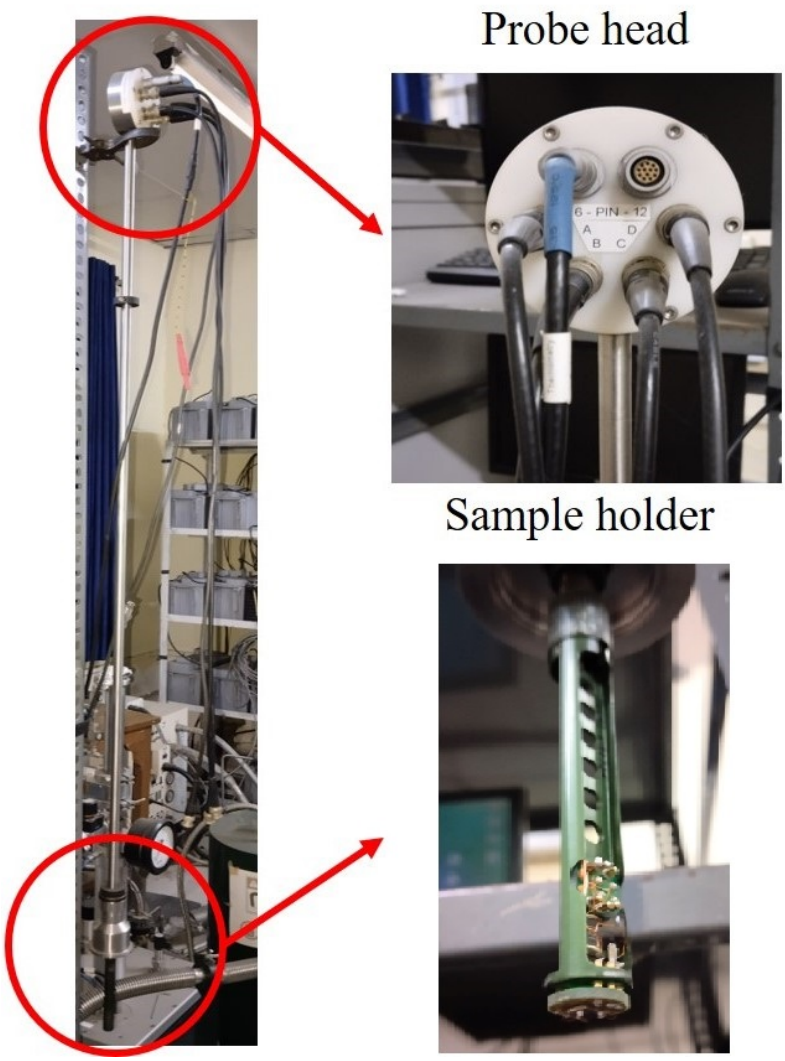

Figure 2.12: The actual image of variable temperature insert with a zoomed view of the probe head and sample holder.

up to atmospheric pressure 3-4 times and then evacuate it to improve the vacuum. After that, to start cooling down, we filled the helium up to a pressure of 0.25 bar and started the compressor meanwhile, we maintained the VTI chamber pressure between 10-15 mbar using the needle valve. In the whole process, the cryostat chamber is continuously put on evacuation to make a thermal insulating environment around the cryostat. The compressed helium cooled down both the VTI chamber and the superconducting magnet, where the temperature decreased gradually, and after 11-12 hours, generally achieved the lowest temperature $\sim$1.4 K, while the magnetic field up to $\pm$7 T can be applied. After getting the low temperature, we start the transport/resistivity measurement.

The resistivity measurement was performed by using a Keithley nanovoltmeter (model no. 2182A) and Keithley constant current (model no. 6221 DC and AC) source, the actual images of these

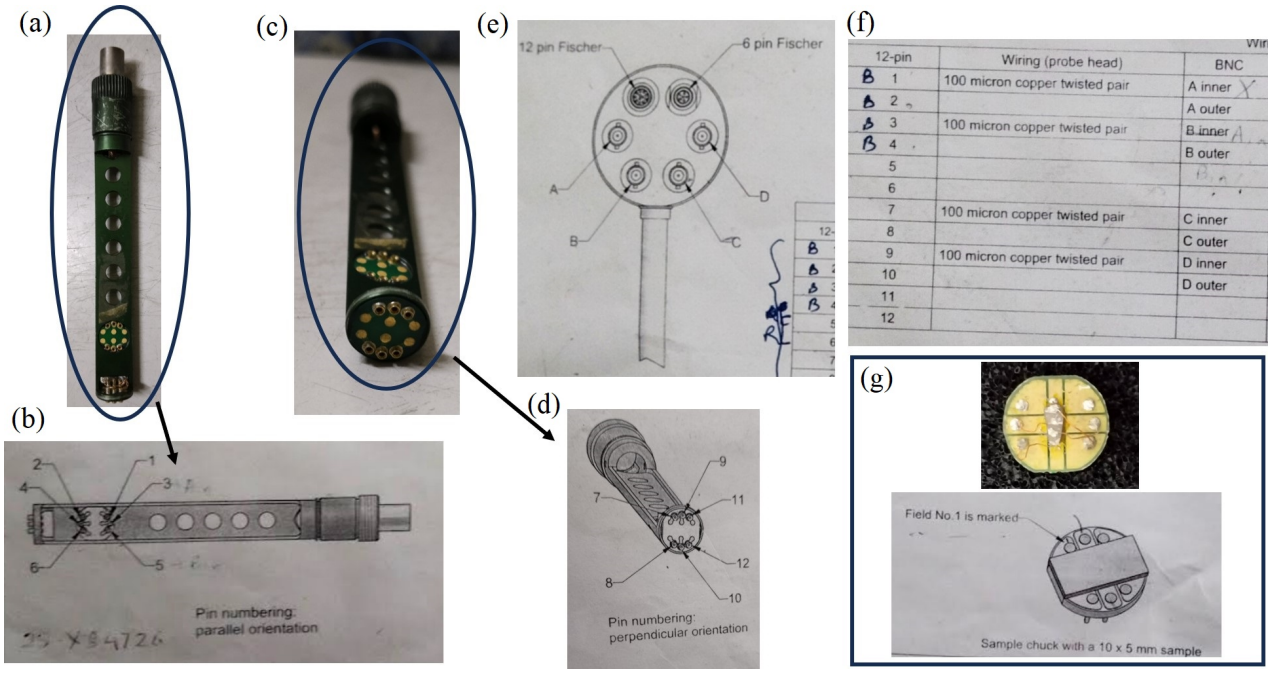

12-pin	Wiring (probe head)	BNC
1	100 micron copper twisted pair	A inner
2		A outer
3	100 micron copper twisted pair	B inner
4		B outer
5		
6		
7	100 micron copper twisted pair	C inner
8		C outer
9	100 micron copper twisted pair	D inner
10		D outer
11		
12		

Figure 2.13: (a) Actual image of the sample holder in parallel orientation. (b) Schematic of sample holder in parallel orientation taken from the manual of the CFMS. (c) Actual image of the sample holder in perpendicular orientation. (d) Schematic of sample holder in perpendicular orientation taken from the manual of the CFMS. (e) Schematic of probe head, taken from the manual of the CFMS. (f) Table shows which pin of the sample holder is connected to which Bayonet Neill–Concelman (BNC) pin of the probe head. (g) Actual and schematic image of the sample puck.

systems are shown in Fig. 2.11 (b) and (c), respectively. Fig. 2.12 is the actual image of VTI rod with a zoomed view of the probe head and sample holder. The Bayonet Neill–Concelman (BNC) pins of the probe head are used to connect the external instruments with the sample that is placed inside the cryostat for measurement purpose. The data from the instruments are acquired by using the LabVIEW programming language. This programming fully automates system operations and runs a wide range of measurements without being present in the laboratory. Initially, we have only the facility to perform longitudinal magnetoresistance measurement (the magnetic field is applied in the direction of current). Therefore, we planned to develop Hall measurement and transverse magnetoresistance (the magnetic field is applied perpendicular to the direction of current) setup in the CFMS.

2.4.1.1 Instrumentation for Hall and transverse magnetoresistance measurements in the CFMS

Fig. 2.13 (a) and (b) represents the actual and schematic image, respectively, of the pin arrangement on the sample holder in parallel orientation. The parallel orientation is used for longitudinal magne-

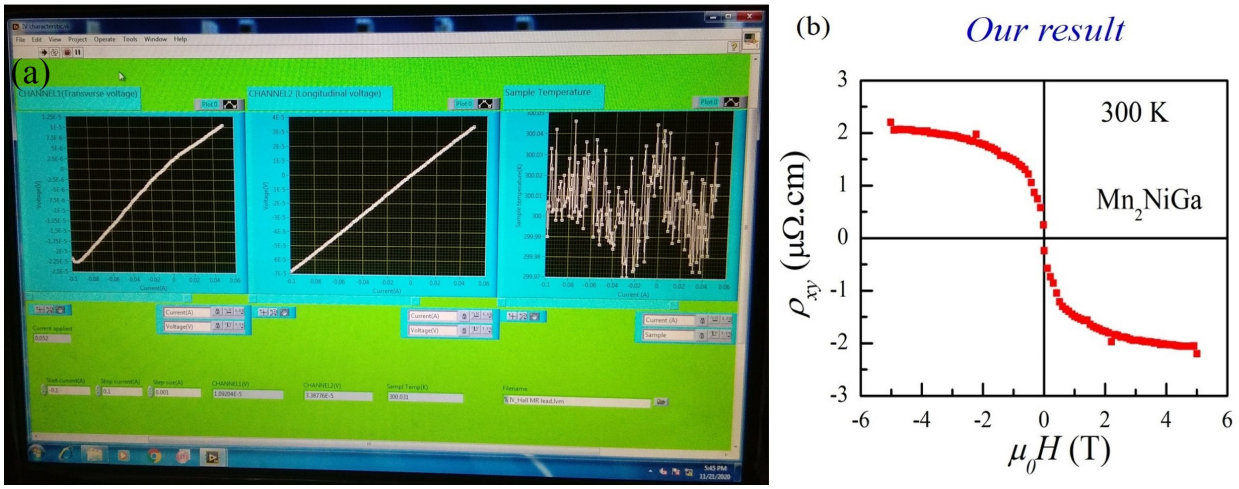

Figure 2.14: (a) Front panel of LabVIEW programming to measure IV characteristics of sample. (b) Hall data of the Mn_2NiGa compound after a number of optimizations.

toresistance measurement, for which the magnetic field should be parallel to the current direction. Fig. 2.13 (c) and (d) show the actual and schematic image of the pin arrangement on the sample holder in perpendicular orientation. Fig. 2.13 (e) depicts the schematic of the probe head with the BNC pin arrangement. The sample holder pins are connected to the BNC pins via an internal copper wire within the VTI rod [Fig. 2.12]. Table in Fig. 2.13 (f) indicates that which pin of the sample holder is connected to which BNC pin of the probe head. The actual and schematic image of the puck where we mount the sample by using GE varnish, is shown in Fig. 2.13 (g). This puck allows sample of maximum size 10×5 mm.

To develop Hall as well as transverse magnetoresistance (MR) measurement setup, instead of the parallel orientation [Fig. 2.15 (a)] we have used the perpendicular one of sample holder [Fig. 2.15 (b)], for which the magnetic field would be perpendicular to the sample plane or current direction. Transverse MR is acquired by measuring the voltage along the direction of current after preparing a four-probe arrangement of indium contact on the sample, as shown in Fig. 2.15 (c). This four-probe geometry eliminates the effects of lead contact resistance from the measurement results, which is the main drawback of the two-probe method. We have observed nice MR data for the Mn_2NiGa compound, as shown in Fig. 2.15 (d). However, the Hall resistivity calculated by measuring the voltage transverse to the applied current direction, have sinusoidal fluctuations. The indium contact arrangement and the collected Hall data are shown in Fig. 2.15 (e) and Fig. 2.15 (f), respectively. Such fluctuations are generally caused by the noise coming from the environment as well as the

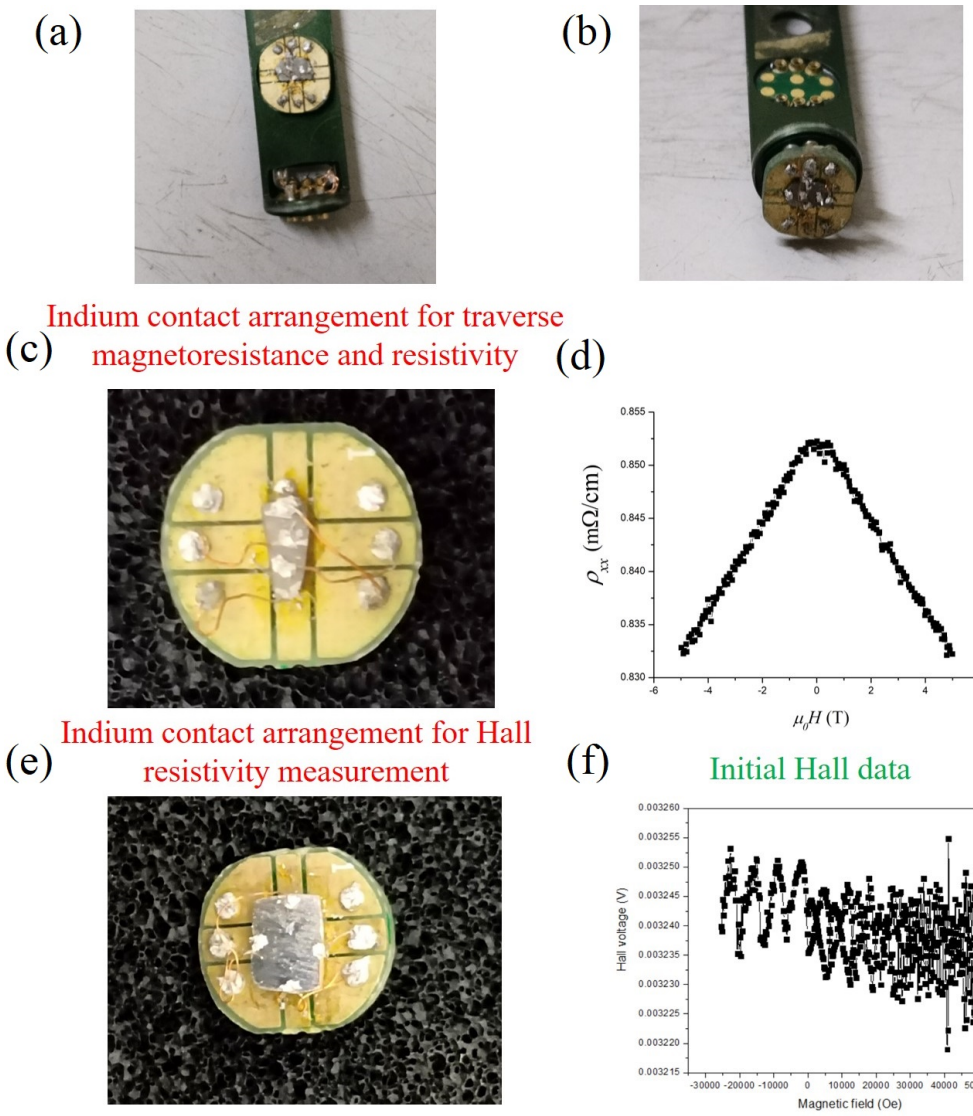

Figure 2.15: (a) Puck with the sample placed in the parallel orientation of the sample holder. (b) Puck with the sample placed in the perpendicular orientation of the sample holder. (c) Contact arrangement for transverse magnetoresistance (MR) measurement. (d) The transverse MR data for Mn_2NiGa compound. (e) Contact arrangement for Hall measurement. (f) The observed Hall data.

instrument itself. This kind of fluctuations that we observed in the Hall data, are not detected in the MR data because the MR signal has a magnitude typically in the order of mΩ.cm, whereas the Hall signal has significantly less magnitude typically in the order of $\mu\Omega$.cm or nΩ.cm, which is of the same order as noise signal coming from environment. To nullify the noise signal and collect the pure Hall signal, we have done a number of optimizations and modified the LabVIEW program accordingly.

(a) Front panel for Hall measurement (b) Front panel for magnetoresistance measurement

Figure 2.16: (a) Front panel of LabVIEW programming to measure Hall data. (b) Front panel of LabVIEW programming to measure MR data.

2.4.1.2 Optimizations for the Hall signal

The step-by-step optimizations we have done are as follows-

1- First, we tried to make proper and strong contact of the copper wire with the sample using indium.

2- We have carefully checked whether the contacts are insulating from each other or not by using a multimeter.

3- We anticipated that the fluctuations are coming from the high ramping rate of magnetic field. Therefore, we performed the magnetic field-dependent measurement with slow ramping rate.

4- The thermal heating caused by the applied current may also give rise to the fluctuation, so we have collected data by changing the current between 10 mA to 150 mA.

5- To check the ohmic contact of the sample with copper wire and temperature stability inside the chamber, we have further developed a LabVIEW program to measure the I-V characteristic of the sample and the temperature of sample with respect to time during magnetic field-dependent measurement, respectively. The front panel of the LabVIEW program is shown in Fig. 2.14 (a). The first window of Fig. 2.14 (a) shows non-ohmic contact (non-linear behavior of V with respect to I), whereas the second window indicates ohmic contact (linear behavior of V with respect to I). The perfect contact will be ohmic and exhibits linear I-V. The third window of Fig. 2.14 (a) is the front panel for measuring the temperature of the sample as a function of time during the field-dependent

measurement.

6- We made some changes in the available LabVIEW programming for the longitudinal MR measurement. We modified the program such that we may apply the DC current (I) in both polarity (+I and -I) across the sample and measure the corresponding voltage (+V and -V). After that, we averaged out the voltage $\left[\frac{(+V)+(-V)}{2}\right]$ to nullify the noise contributions from the environment and the instrument itself. This averaging is performed a number of times, which leads to a good-quality data point after averaging a bulk of data at a particular temperature or field. Still, the signal has fluctuations, for that, we have reduced the thickness of sample (0.3-0.7 mm depending on the magnitude of the signal). For a good signal, the sample size should be around 6 mm $\times$ 3 mm, and the thickness should be less than 1 mm.

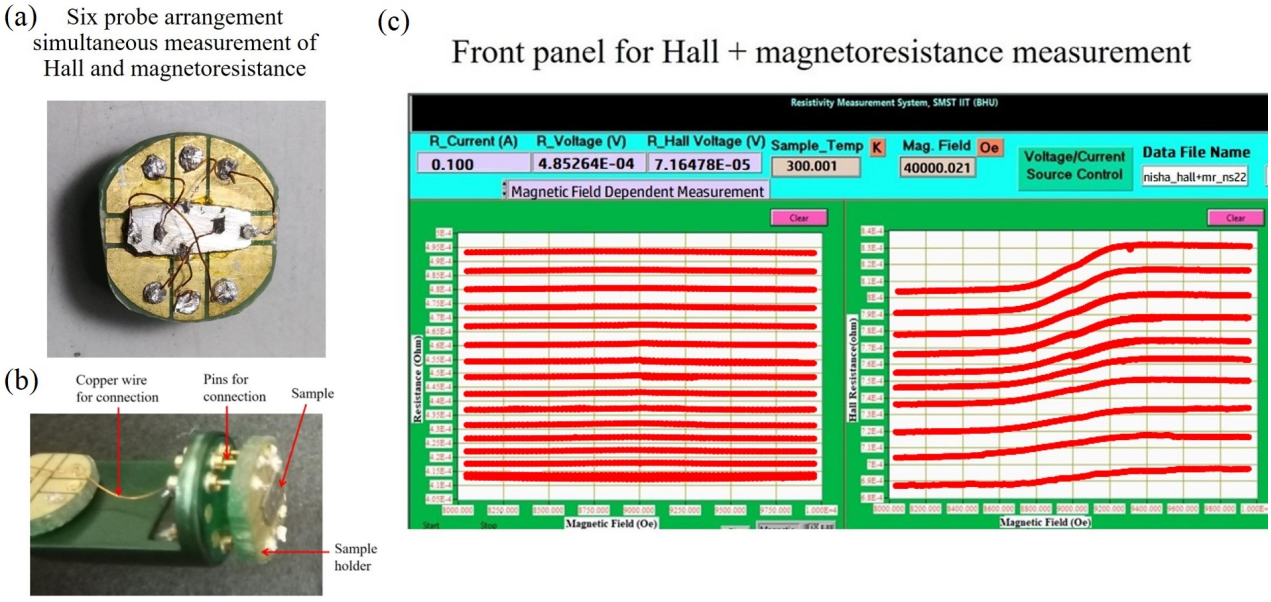

Figure 2.17: (a) Six probe arrangement for simultaneous measurement of Hall and transverse magnetoresistance (MR). (b) Connection of the perpendicular pin with the parallel pin by using copper wire. (c) Front panel of the simultaneous measurement of Hall and transverse MR.

In this way, for a fixed current (around 100 mA), the voltage across the Mn_2NiGa compound has been collected with the change in temperature or magnetic field and then calculated resistance by using Ohm′s law $R = \frac{V}{I}$. The resistivity of the sample is calculated by using the formula $\rho = R \times \frac{A}{l}$, where A and l are the cross-sectional area and length of the sample, respectively. Finally, we got a nice Hall signal [Fig. 2.14 (b)] of the Mn_2NiGa compound, which is well matching with the literature [7]. After optimizations, the front panel of the LabVIEW program to acquire the Hall and MR data

are shown in Fig. 2.16 (a) and Fig. 2.16 (b), respectively.

Furthermore, to collect the transverse MR and Hall data simultaneously, we have modified the LabVIEW program by using both channels of the multichannel Keithley nanovoltmeter. For such simultaneous measurement, we have prepared 6 probe contact arrangement on the sample, as shown in Fig. 2.17 (a). The two extra probes are generated by connecting two pins of perpendicular pin arrangement with the two pins of parallel pin arrangement, as shown in Fig. 2.17 (b). The front panel of the LabVIEW program for simultaneous measurement of Hall and transverse MR is shown in Fig. 2.17 (c).

2.4.2 Physical property measurement system (PPMS) with electrical transport option (ETO)

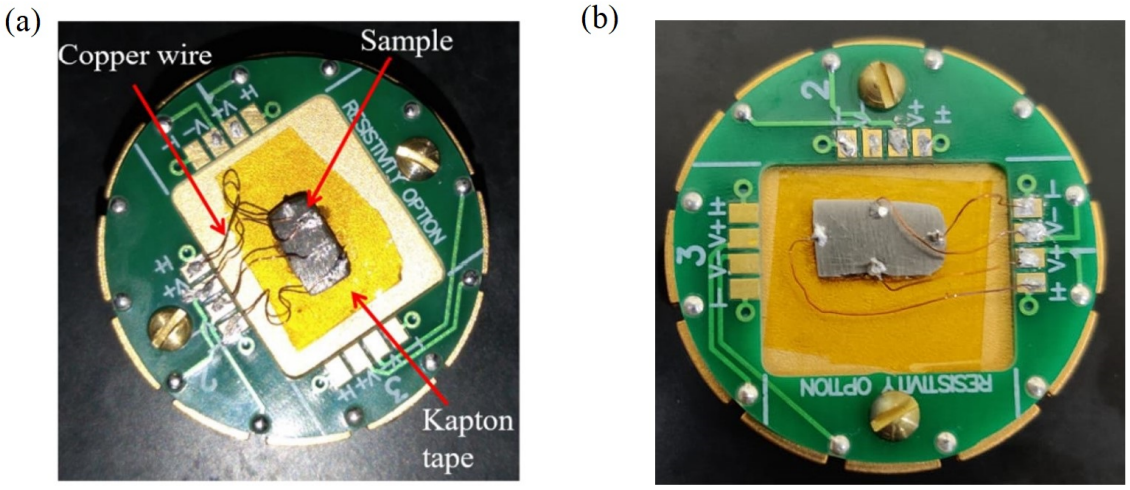

Four probe arrangement for resistivity and magnetoresistance

Four probe arrangement for Hall measurement

Figure 2.18: Four probe arrangement of resistivity, magnetoresistance, and Hall measurement in the physical property measurement system.

Besides the CFMS, electrical transport measurements are carried out by using ETO in the physical property measurement system (PPMS) system of Quantum Design (QD). The resistivity, magnetoresistance, and Hall resistivity of the sample are collected by using the same four-probe method, as shown in Fig. 2.18. In this system, the AC current is used for the transport measurement in contrast to the DC current used in the CFMS system. The sample size should be less than 8 mm $\times$ 4 mm and a thickness of less than 1 mm. The ETO software is integrated into the MultiVu software application

used to control and monitor the system hardware. This software integration allows utilizing MultiVu sequences to fully automate system operations and run a wide range of measurements without being present in the laboratory. The details of the PPMS system are written in the previous section of magnetic measurement.

2.5 Scanning electron microscope (SEM) and energy dispersive analysis of X rays (EDX)

The uniform growth of samples is confirmed by taking the surface image with high resolution down to the sub micron-scale using EVO-Scanning Electron Microscope (SEM) MA15/18 (ZEISS). The elemental identification and quantitative compositional information were collected by the energy dispersive analysis of x-rays (EDAX) technique. The EDAX characterization was performed using an energy dispersive spectroscopy (EDS) detector (Model No.51N1000-EDS System) attached to the SEM.

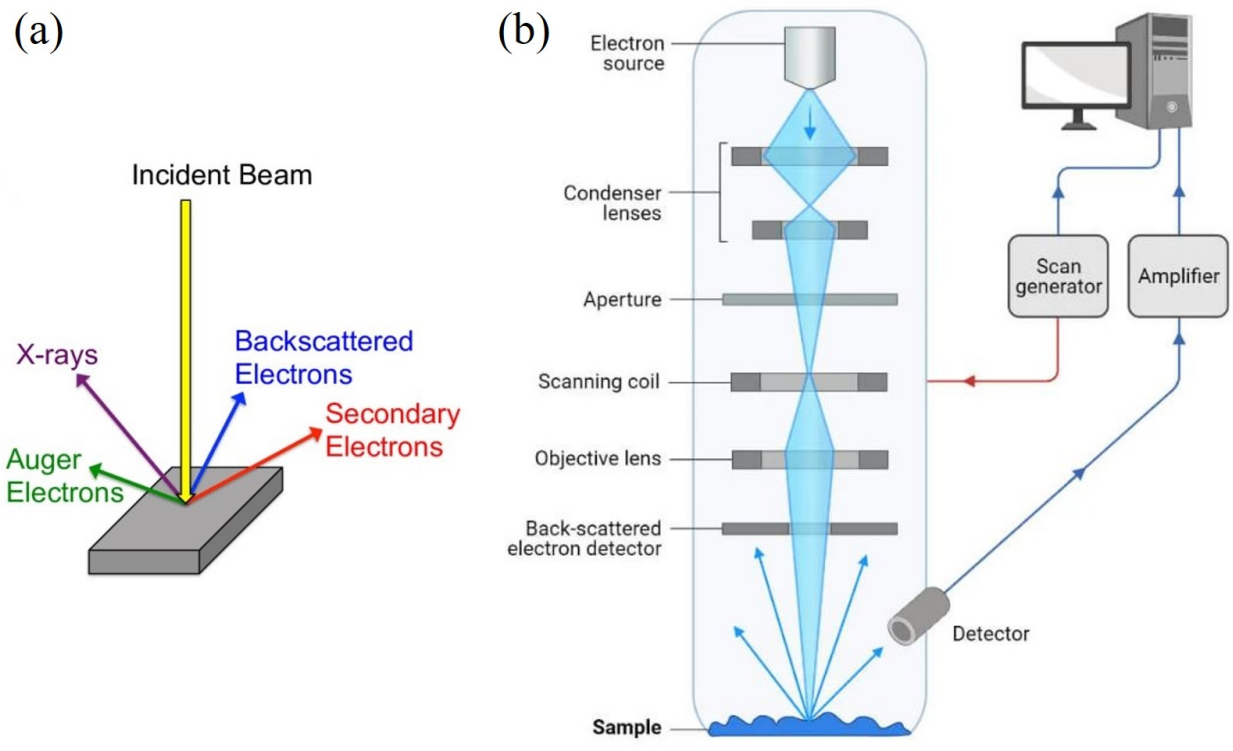

Figure 2.19: Schematic diagram of the sample-beam interactions within a scanning electron microscope [8, 9].

The SEM is a microscope that uses electrons instead of light to collect an image. Electron microscopes have very short wavelengths in comparison to the light microscope, which enables better resolution power. As the highly energetic electrons interact with the sample, they produce secondary electrons, backscattered electrons, and characteristic X-rays, as shown in Fig 2.19 (a).

The secondary electrons, backscattered electrons signals, are collected by detectors to form images which are then displayed on the computer screen. The characteristic X-rays are generated according to the characteristics and nature of the elements present in the sample. Hence, this technique also can be used to measure the energy of emitted X-rays for the purpose of elemental analysis. When the electron beam hits the surface of the sample, it penetrates the sample to a depth of a few microns, depending on the accelerating voltage and the density of the sample.

SEM consists of different major components such as an electron source, electromagnetic lenses, scanning coil, detector, computer, power supply, vacuum, and cooling system, as shown in Fig. 2.19 (b). The electron source is used to emit electrons under thermal heat at a voltage of 1-40 kV. There are three types of electron sources that can be used, i.e., tungsten filament, lanthanum hexaboride, and field emission gun (FEG).

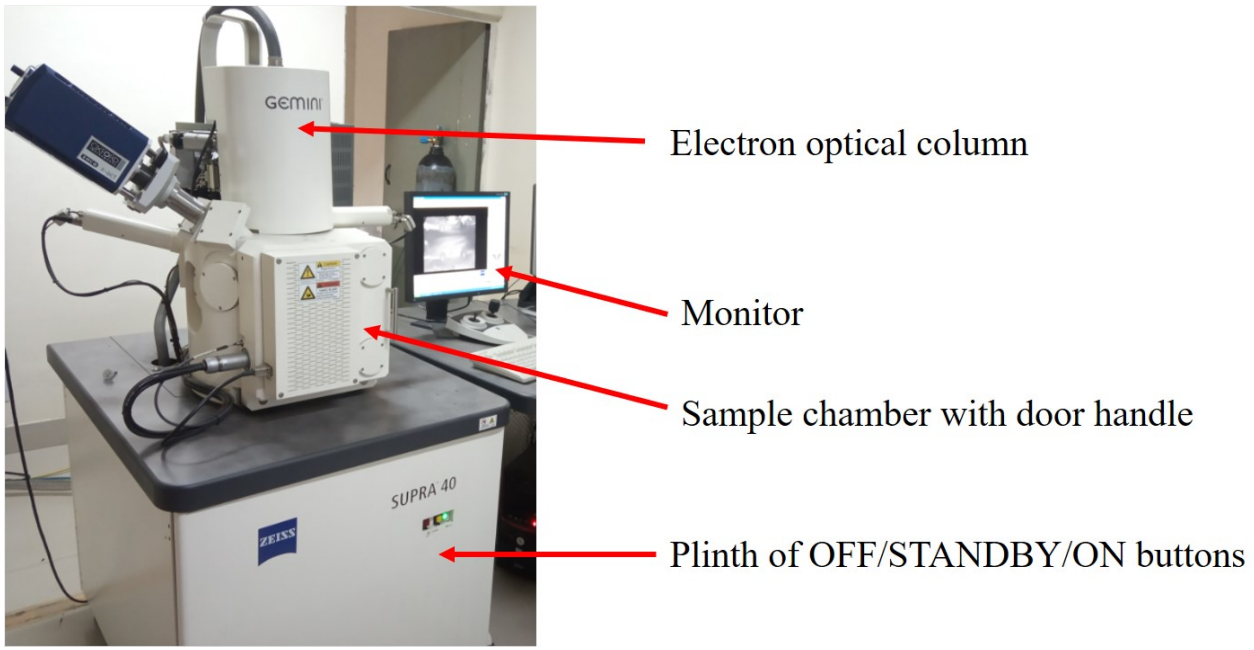

Figure 2.20: Actual image of scanning electron microscope at School of Materials Science and Technology, IIT (BHU).

Several electromagnetic lenses, named condenser lenses, are used to focus the beam of electrons

from the source through the column, forming a narrow beam of electrons that form a spot called a spot size. Scanning coils are used to deflect the electron beam. When electrons interact with the sample, they produce different signals directed toward the detector, which is made up of several detectors that are able to differentiate the secondary electrons, back-scattered electrons, and characteristic x-Rays. These signals are displayed on the computer. The vacuum systems, such as turbo and rotary pumps are used to create a vacuum environment in the electron gun source and sample chamber, etc. A cooling system, such as a water chiller is used for dumping excessive heat from the electron source. The actual image of SEM is shown in Fig. 2.20.

2.6 X-ray photoelectron spectroscopy (XPS)

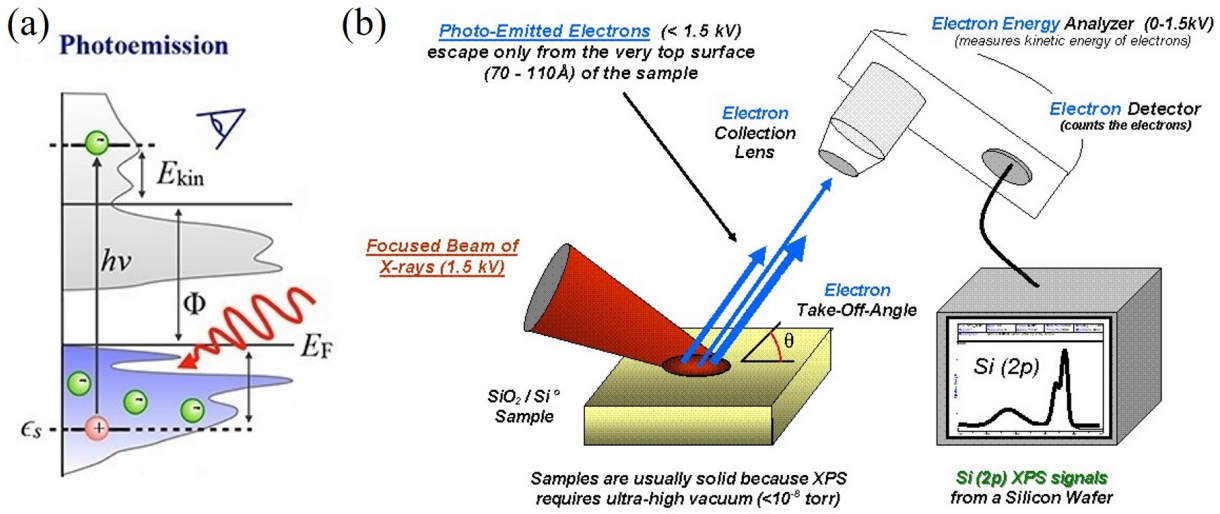

Figure 2.21: (a) Schematic of the photoemission [10]. (b) Basic components of an x-ray photoelectron spectroscopy system [11].

XPS works on the principle of measuring the kinetic energy of electrons that are emitted from the top 1-10 nm of the sample when a beam of X-rays falls on it. When a photon of well-defined energy ($\hbar\omega$) falls on a sample, it is used to overcome the electron binding energy (E_b) and the work function (ϕ_w) so that the electron is ejected with the remaining kinetic energy (E_{kin}). Therefore, E_{kin} of the ejected photoelectron is given by-

$$E_{kin} = \hbar\omega - E_b - \phi_w \tag{2.5}$$

The number of electrons (I) as a function of E_{kin} gives the photoemission spectrum $I(E_{kin})$, as shown in Fig. 2.21 (a).

XPS is used to identify the elements present in a sample. The XPS is also used to confirm the elemental composition, chemical and electronic states of the elements within the sample. It mainly consists of an x-ray source, an electron energy analyzer, and a computer, as depicted in Fig. 2.21 (b). In the present work, the XPS data is collected by using the K-Alpha x-ray photoelectron spectrometer system from ThermoFisher-scientific with a monochromatized Al anode X-ray source. The collected spectra are analyzed by using open source software XPSPEAK41.

2.7 X-ray absorption near edge spectroscopy (XANES)

The x-ray carries energy (E) that is enough to ionize a core electron of an atom from E_i energy state. Thus, the absorption of x-rays by an atom leads to either excitation of an electron to E_f energy state in the unoccupied state, or it can be ejected from the atom if $E > E_f - E_i$. The spectroscopy based on the former excitation is known as x-ray absorption spectroscopy (XAS), while on the later excitation, it is known as x-ray photoelectron spectroscopy.

After the excitation, a core hole is created; therefore, the atom becomes unstable and tends to relax spontaneously. The hole can be relaxed by filling an electron from the upper level leading to the generation of fluorescence photons, which can be absorbed by the electron resulting in the generation of the Auger electron. These characteristics processes can be detected, and therefore the corresponding XAS spectrum can be measured. The detection of the yield of fluorescence photons is known as the total fluorescence yield (TFY) mode for XAS measurement. However, the Auger electron undergoes a cascade scattering with the atom, which results in the generation of a secondary electron. The detection of the yield of the secondary electron is known as the total electron yield (TEY) mode of measurement. Unlike TFY, TEY mode is sensitive to the surface because of the smaller escape depth of the secondary electron, which is a few nanometers. The TEY and TFY modes of XAS measurements have been widely utilized for thin films.

The XANES region is limited to E_0 + 50 eV. Typical x-ray absorption near edge structure (XANES) region for Fe K-edge is shown in Fig. 2.22. The XANES is an analytical technique used to elucidate

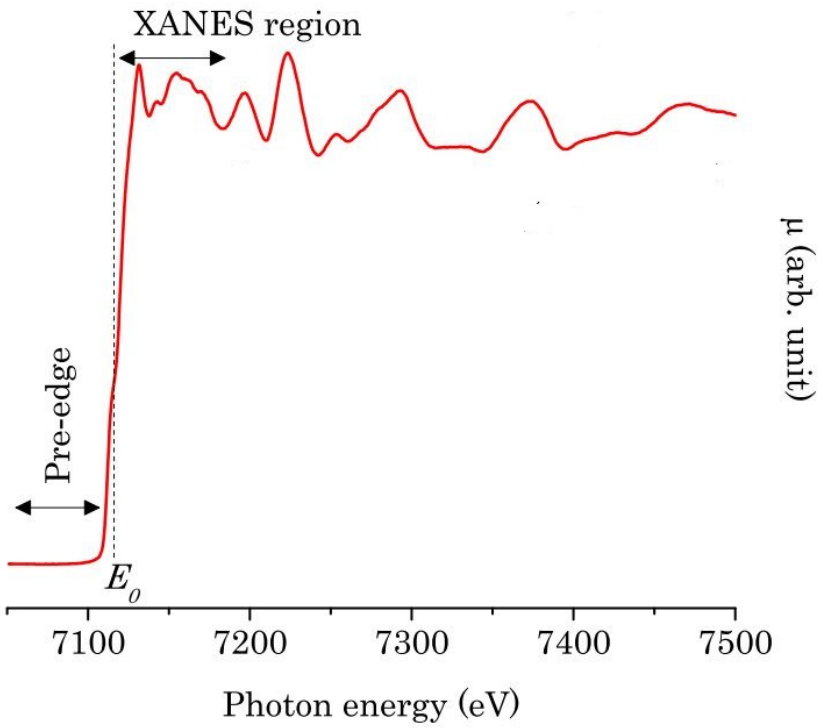

Figure 2.22: X-ray absorption near edge region of Fe K-edge x-ray absorption spectrum [12].

the local electronic structure of an atom. Frequently, this technique is implemented to track changes to the oxidation state elements in actual-time. In addition, the lowest energy feature in the XANES spectrum arises just below the sharp absorption edge. This region is commonly known as the pre-edge region. The intensity of pre-edge features is affected by the symmetry of the local environment around the absorbing atom.

The XANES measurements have been carried out at the BL-01 beam line of the Indus-2 synchrotron Radiation Source. The experimental setup for XAS measurements at the BL-01 beamline of the Indus-2 synchrotron source is shown in Fig. 2.23. The experimental setup consists of a synchrotron radiation source that operates at the electron energy of 2.5 GeV and a current of 150 mA. The source is capable of producing high-brilliance of x-rays with a tunable range of energy. A broad beam from the synchrotron source falls on a toroidal pre-mirror (TPM) M1 after passing through a polarization section aperture (PSA). Using the PSA, one can also perform x-ray magnetic circular dichroism experiment at this beam line. The TPM performs vertical focusing of the synchrotron beam at the entrance slit and horizontal focusing at the exit slit. After passing from TPM, the beam falls on a spherical grating monochromator (SGM) through an entrance slit; the SGM selects x-rays of desired

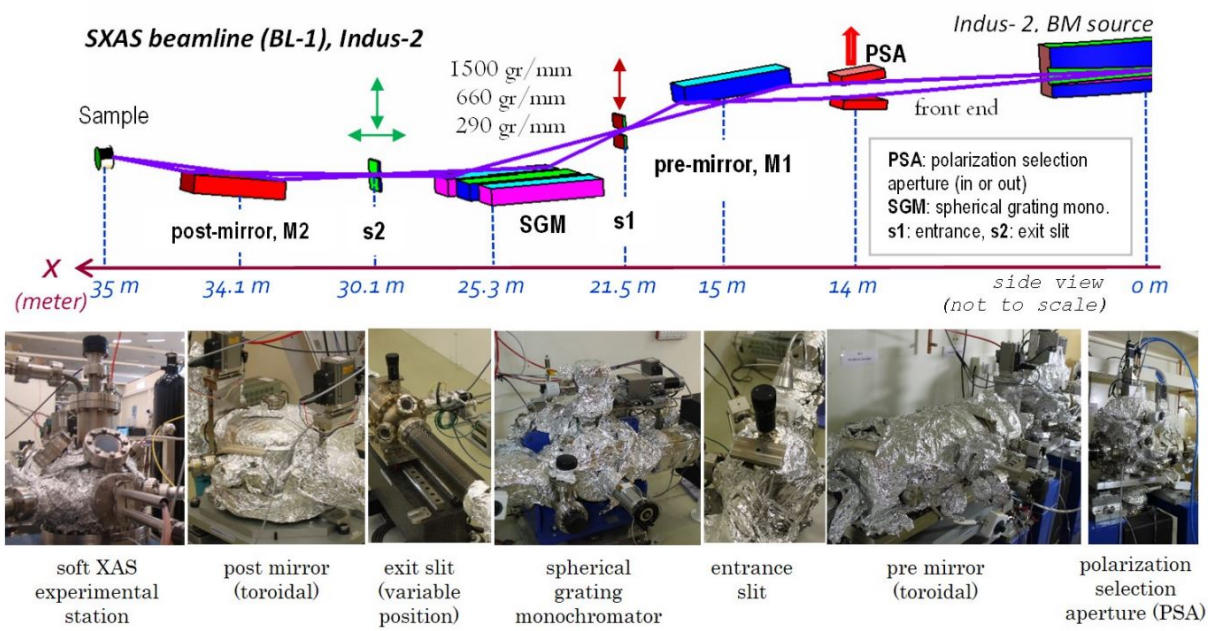

Figure 2.23: Experimental setup for x-ray absorption spectroscopy measurement at the BL-01 beam line of Indus-2 synchrotron Radiation Source at RRCAT Indore.

energy. In this setup, three SGM are used to select x-rays of energy between 100- 1200 eV. The SGM also performs horizontal focusing of the beam. After passing from the SGM, the beam falls on a post mirror through an exit slit that focuses the beam on the sample. The various components of the beam line, such as entrance slit and exit slit width, PSA position, and SGM movement for the selection of x-rays of varying energy, can be controlled by computer software written in LabVIEW graphical programming language.

2.8 X-ray reflectometry (XRR)

XRR is a non-destructive and surface-sensitive analytical technique used in materials science to characterize surfaces, thin films, and multilayers. It is a grazing incident scattering technique that uses an x-ray beam, incident on a flat surface at very low angles (0.2- 3^o).

The basic principle of X-ray reflectivity is to reflect the beam of X-rays from the flat surface and then measure the intensity of X-rays reflected in the direction of an angle equal to the incident angle, as depicted in Fig. 2.24 (a). X-ray reflectivity measurements are analyzed by fitting the collected data using the recursive Parratt′s formalism combined with the rough interface formula. The fit-

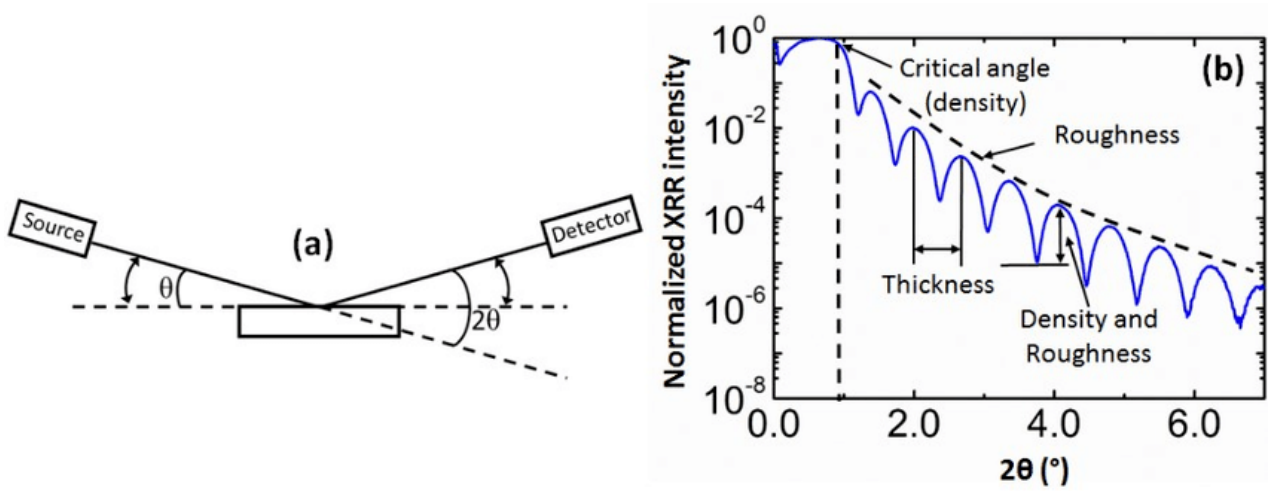

Figure 2.24: (a) Schematic of x-ray reflectometry (XRR) measurement geometry. (b) Example of XRR spectrum [13].

ting parameters are typically layer thicknesses, densities, and interfacial roughnesses [Fig. 2.24 (b)], which are obtained by performing the fitting of the data using the open-source software Prratt32. In the present work, the XRR data is collected by using an x-ray source of Bruker D8 Discover.

References

[1] P. N. Hishimone, H. Nagai, and M. Sato, Methods of Fabricating Thin Films for Energy Materials and Devices, Lithium-ion Batteries - Thin Film for Energy Materials and Devices. IntechOpen, (2020).

[2] M. Eckert, Disputed discovery: The beginnings of X-ray diffraction in crystals in 1912 and its repercussions. Z. Kristallogr. **227**, 27–35 (2012).

[3] Britannica, The Editors of Encyclopaedia. ”Bragg law”. Encyclopedia Britannica, 15 Mar. 2022, https://www.britannica.com/science/Bragg-law. Accessed 28 May (2023).

[4] S.K. Ali, U. Das, Y. Lu, V. Kundapur, T. May, Synchrotron Radiation: Applications in Diagnosis and Treatment of Malignant Brain Tumors, Diagnostic techniques and surgical management of brain tumors, IntechOpen (2011).

[5] A.-C. Dippel, H.-P. Liermann, J.T. Delitz, P. Walter, H. Schulte-Schrepping, O.H. Seeck, H.

Franz, Beamline P02.1 at PETRA III for high-resolution and high-energy powder diffraction, Journal of synchrotron radiation, **22** 675-687 (2015).

[6] R.B. Vibrating Sample Magnetometer (VSM) Option User's Manual, Quantum Design, 1096-100 (2011).

[7] S. Sen, C. Singh, P. K. Mukharjee, R. Nath, and A. K. Nayak, Observation of the topological Hall effect and signature of room-temperature antiskyrmions in Mn-Ni-Ga D_{2d} Heusler magnets. Phys. Rev. B **99**, 134404 (2019).

[8] M. J. Walock. Nanocomposite coatings based on quaternary metalnitrogen. Other. Ecole nationale sup´erieure d'arts et m´etiers - ENSAM, 2012. French.

[9] https://microbenotes.com/scanning-electron-microscope-sem/.

[10] D. Golze, M. Dvorak, P. Rinke, The GW Compendium: A Practical Guide to Theoretical Photoemission Spectroscopy, Frontiers in Chemistry **7**, (2019).

[11] https://en.wikipedia.org/wiki/X-ray$_$photoelectron$_$spectroscopy.

[12] L. M. Mottram, S. Cafferkey, A. R. Mason, T. H. Oulton, S. Sun, D. J. Bailey, M. C. Stennett, N. C. Hyatt, A feasibility investigation of speciation by Fe K-edge XANES using a laboratory X-ray absorption spectrometer, Journal of Geosciences **65** 27-35 (2020).

[13] R.C. Ribera, Growth and thermal oxidation of Ru and ZrO_2 thin films as oxidation protective layers. [PhD Thesis - Research UT, graduation UT, University of Twente]. Universiteit Twente. (2017).